Non-equilibrium solidification and ferrite in δ-TRIP steel

H. L. Yi[1], S. K. Ghosh[1], W. J. Liu[1], K. Y. Lee[2] and H. K. D. H. Bhadeshia*[1,3]

Microscopy and microanalysis experiments on two cast alloys, designed on the basis of equilibrium to contain substantial amounts of δ-ferrite, reveal zero or much reduced fractions of this phase in the solidified condition. It appears that the solid state transformation of δ-ferrite into austenite occurs without the required partitioning of solutes and that this is responsible for the development of non-equilibrium microstructures. This conclusion is supported by microanalytical data and through calculations of limiting phase diagrams based on paraequilibrium rather than equilibrium. Kinetic simulations confirm that this interpretation is consistent with the majority of austenite growing in the solid state without the partitioning of the substitutional solutes.

Keywords: δ-TRIP steel, TRIP, Steel, Paraequilibrium

Introduction

Transformation induced plasticity (TRIP) assisted steels contain allotriomorphic ferrite as the major phase, with the rest of the microstructure consisting of carbide free bainitic ferrite and carbon enriched retained austenite.[1–10] An unconventional TRIP assisted steels has recently been invented, designated δ-TRIP,[11] because the usual allotriomorphic ferrite grains are replaced by dendritic δ-ferrite, which grows from the liquid steel. Furthermore, the δ-ferrite persists at all temperatures and cannot be removed by heat treatment because it is a thermodynamically stable phase. Otherwise, the residual microstructure in the interdendritic regions is still the same, consisting of a mixture of bainitic ferrite with enriched austenite.

The steel has interesting properties: an ultimate tensile strength in the as cast condition of about 1000 MPa and a total elongation, almost all of which is uniform, of 23%. It has been demonstrated that the combination of strength and ductility is due partly to the deformation induced transformation of the retained austenite into martensite, resulting in an enhanced resistance to plastic instabilities.[11]

The alloy contains only 0·5 wt-% of silicon in order to avoid surface quality and galvanising problems.[1,12,13] However, one role of the silicon is to stop the precipitation of cementite during the bainite reaction,[14–17] and 0·5 wt-% can be insufficient to achieve this.[13] To cope with this difficulty, δ-TRIP also contains aluminium, which is known to retard the precipitation of cementite[18–20]; the aluminium also helps to ensure the presence of δ-ferrite during the solidification phase.

The presence of δ-ferrite is crucial in this novel system, and the authors' experiments have indicated that its occurrence is temperamental and sometimes inconsistent with what is expected at thermodynamic equilibrium. Non-equilibrium solidification and any consequences of this on solid state transformation could play an important role in the management of the microstructure. Thus, the goal of the work presented in this paper was to study the vagaries of the formation of ferrite during solidification in the context of δ-TRIP steel.

Alloy design and manufacture

Based on previous work,[11] two alloys were designed with different aluminium concentrations (Table 1). The details of the design method and the role of each solute have been discussed in Ref. 11, but the essence of the procedure is that a microstructure containing δ-ferrite as the majority phase in the form of dendrites is desired. Thermodynamic phase diagrams were estimated using MTDATA[21] in combination with the TCFE (version 1·21) database. The alloys were manufactured as 34 kg ingots of $100 \times 170 \times 230$ mm dimensions using a vacuum furnace. Optical microscopy samples were prepared using standard methods and etched in 2% nital. Higher resolution observations and energy dispersive X-ray microanalysis were done using a field emission scanning electron microscope operating at 10 kV accelerating voltage.

The calculated equilibrium phase diagrams for the manufactured alloys are presented in Fig. 1*a* and *b*. The figure shows that under equilibrium conditions, the minimum amount of ferrite to be expected in the microstructure is 35 and 51 wt-% for alloys 1 and 2. Furthermore, both alloys start solidification with δ-ferrite, which remains the only solid phase until most of the liquid has been consumed. The few percentage of liquid that remains (henceforth referred to as the

[1]Graduate Institute of Ferrous Technology (GIFT), Pohang University of Science and Technology (POSTECH), Pohang 790-784, Korea
[2]POSCO Technical Research Laboratories, Gwangyang-si, Jeonnam, Korea
[3]Department of Materials Science and Metallurgy, University of Cambridge, Pembroke Street, Cambridge CB2 3QZ, UK

*Corresponding author, email hkdb@cam.ac.uk

Published by Maney on behalf of the Institute
Received 26 July 2008; accepted 2 March 2009
DOI 10.1179/174328409X428918

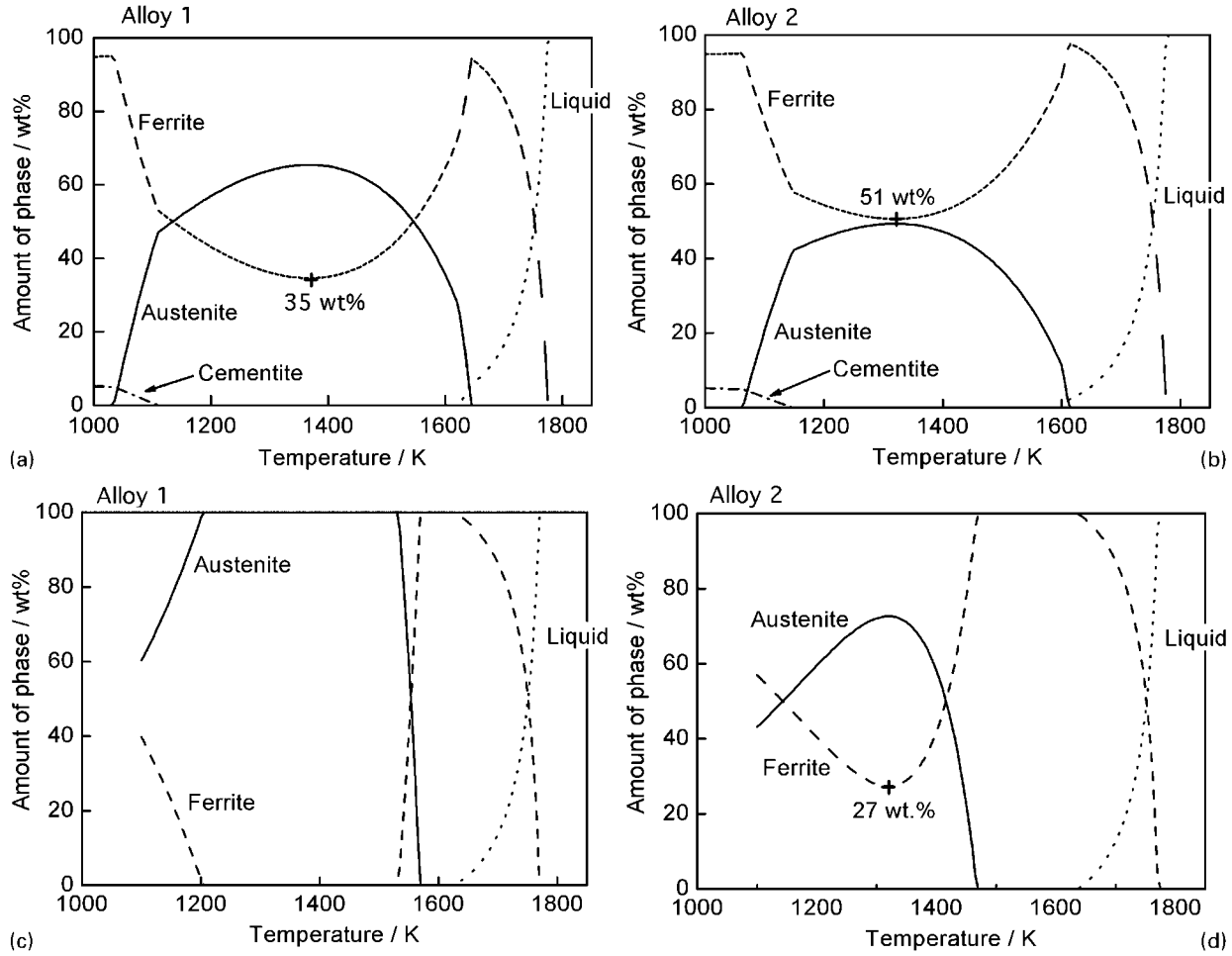

a, *b* equilibrium data; *c*, *d* paraequilibrium data

1 Calculated phase fractions as function of temperatures and alloy

residual liquid) then converts into austenite, which, on cooling, continues to grow in proportion by consuming the δ-ferrite.

Metallography

The optical microstructures of alloy 1 in the cast condition shows the remnants of the dendritic solidification process through coring effects, but the δ-ferrite dendrites themselves are completely absent (Fig. 2*a*). Instead, the microstructure has evolved, with the δ-ferrite transforming completely into austenite, which itself then transforms into a small amount of allotriomorphic and Widmanstätten ferrite but predominantly into pearlite and on cooling. This is quite inconsistent with the phase calculations in Fig. 1*a*, which indicate that, under equilibrium conditions, as a minimum, some 35 wt-% of the microstructure should consist of δ-ferrite.

The microstructure in the cast condition for alloy 2 is more as expected, with prominent dendrites of δ-ferrite and pearlite resulting from the solid state transformation of austenite (Fig. 2*c*). However, even in this case, the total amount of δ-ferrite is much less than the minimum of 51 wt-% indicated by the phase diagram calculations in Fig. 1*b*. Indeed, the total ferrite content (δ and α) is expected to be much higher on reaching ambient temperature.

It is likely that solidification occurs under conditions which deviate from equilibrium. The solutes, particularly those that are substitutional, may not in such circumstances partition to the fullest extent required by thermodynamic equilibrium. To assess this, paraequilibrium phase diagrams were calculated using MTDATA, although it is emphasised that it is not yet possible, due to a lack of thermodynamic data, to include cementite in such calculations. Paraequilibrium is a state of constrained equilibrium in which the substitution to iron atom ratio is maintained constant everywhere, but subject to this constraint, the carbon partitions, to achieve a uniform chemical potential.[22–28] The results are shown in Fig. 1*c* and *d*, where it is evident that under paraequilibrium conditions, alloy 1 can become fully austenitic and that the minimum quantity of δ-ferrite possible in alloy 2 could be dramatically reduced.

Table 1 Design compositions and those actually achieved during manufacture, wt-%

	Alloy 1		Alloy 2	
	Design	Actual	Design	Actual
C	0·4	0·36	0·4	0·37
Si	0·25	0·26	0·25	0·23
Mn	2·0	2·02	2·0	1·99
Al	2·1	2·13	2·5	2·49
Cu	0·5	0·49	0·5	0·49
P	0·02	0·02	0·02	0·02
S		0·0033		0·0036
N		0·0048		0·0048

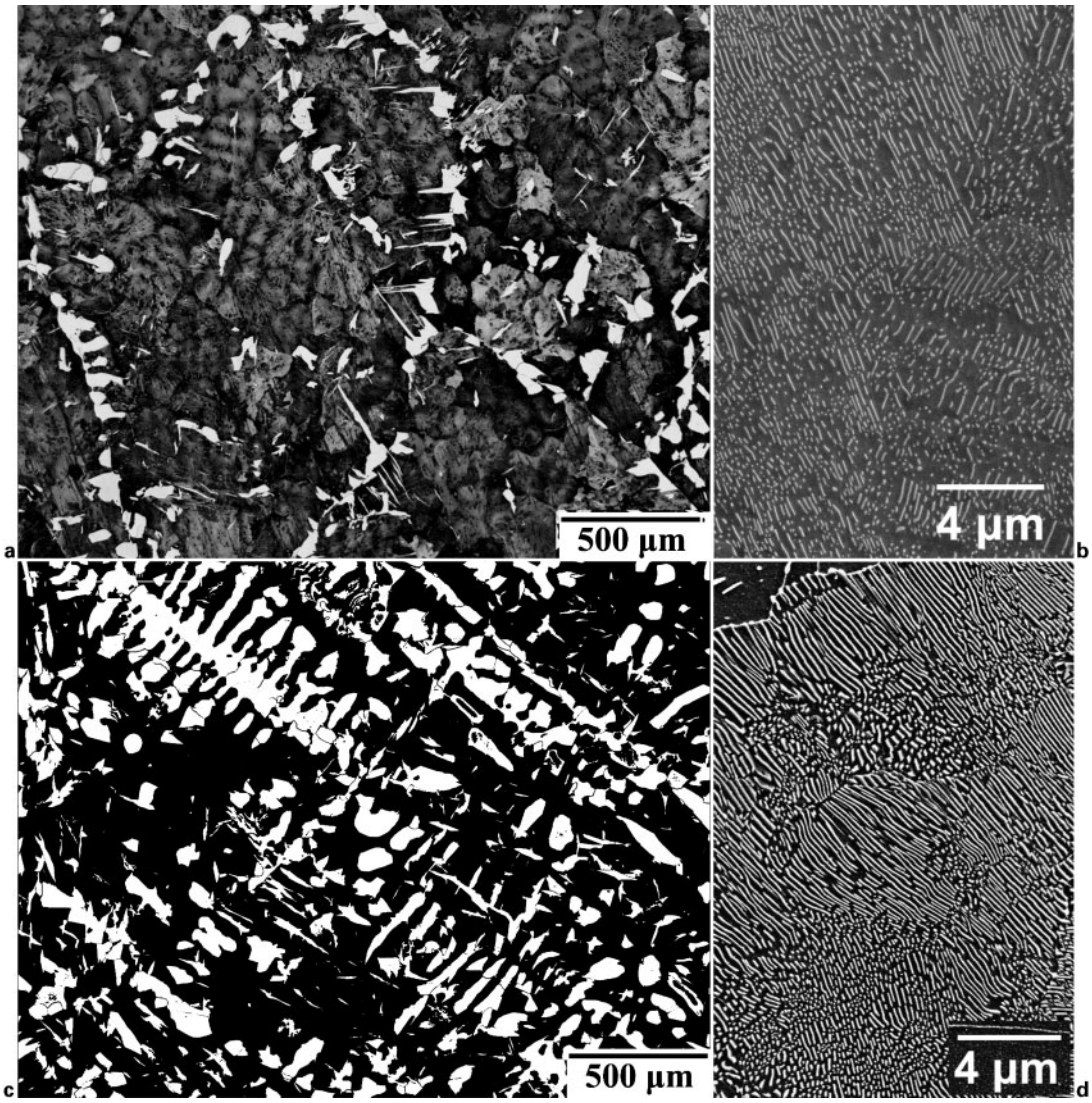

a general microstructure of alloy 1; *b* higher magnification image of dark areas of alloy 1 showing pearlite; *c* general microstructure of alloy 2; *d* higher magnification image of dark areas of alloy 2 showing pearlite

2 Microstructure of cast alloys: dark regions are fine pearlite and white, ferrite

It is worth commenting on the pearlite obtained in both alloys, given that the fraction of pearlite is much larger than might be expected from the amount of carbon (<0·4 wt-%) in the steels. Clearly, the volume fraction of cementite within the pearlite must be about half that in a eutectoid steel. A careful examination of Fig. 2*b* and *d* shows that the cementite is discontinuous in most locations rather than present as neat lamellae alternating with ferrite. This is a consequence of the low carbon concentration.

Microanalysis

Full equilibrium data[21] for the key solutes are presented in Fig. 3, both to illustrate the partitioning behaviour and to form the basis for the comparisons with measurements.

The real state of solidification with respect to the substitutional solutes is likely to be between equilibrium and paraequilibrium (an infinite number of intervening states is possible). Microanalysis experiments were conducted to assess the fine scale distribution of solutes between the dendrites and interdendritic spaces where austenite initiates. These experiments were not conducted on alloy 1 where the δ-ferrite dendrites were not present in their original state in the final microstructure. The discussion focuses on the major substitutional solutes Mn and Al, but the interpretations are consistent with the behaviour of the minor solutes, with the exception of carbon, which cannot be determined quantitatively with the microanalysis technique used.

The locations where microanalysis experiments were carried out are illustrated in Fig. 4; the intention was to measure the composition of the δ-ferrite dendrites in general and that of austenite at two locations. The latter is necessary because there are effectively two kinds of austenite, that which forms from the liquid residue left after δ-ferrite and the second type which grows by solid state transformation as it consumes the δ-ferrite. Thus, locations 2 and 3 in Fig. 4*b* correspond to austenite from solid, whereas location 4 is at the core of the austenite, i.e. which originated from interdendritic liquid.

The results, quantitatively listed in Table 2 and plotted in Fig. 5, show that the composition of δ-ferrite corresponds essentially to that expected from equilibrium at the temperature (1612 K), where solidification

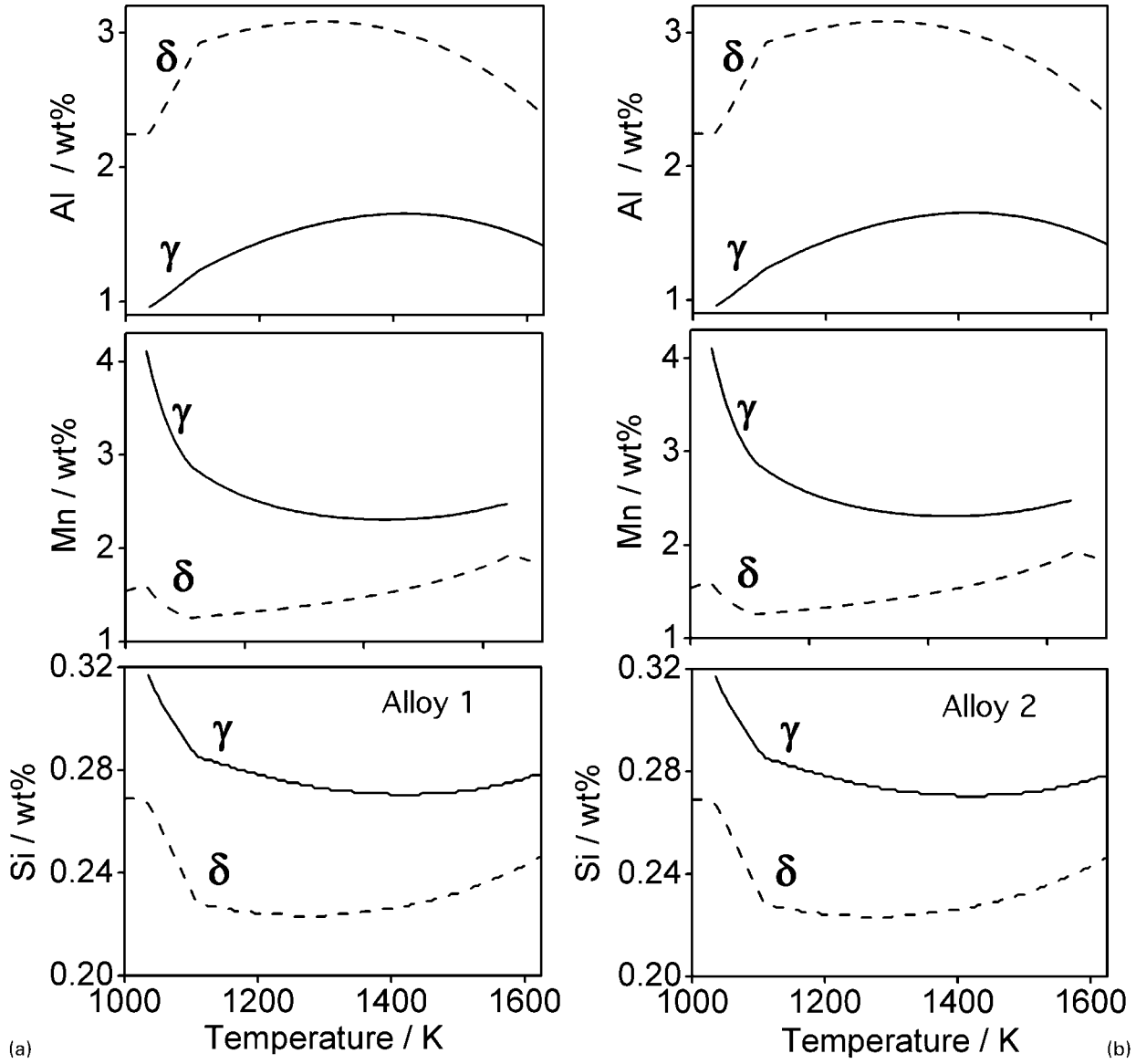

3 Calculated equilibrium compositions of phases as function of temperature

is almost complete and austenite formation from liquid commences. Not surprisingly, the austenite that forms from the residual liquid is rich in Mn and depleted in Al, consistent with the equilibrium calculations. This is not the case for the austenite that grows in the solid state, which inherits the concentrations in the δ-ferrite.

In summary, the composition of the δ-ferrite ceases to change significantly during cooling following solidification, and much of the austenite evolves by growing into the δ-ferrite without the partitioning of substitutional solutes, i.e. by a process which may not be far from paraequilibrium. Figure 6 shows the same effect more vividly as a scan across the core of an austenite region. These results explain why the expected quantities of δ-ferrite are not obtained in contradiction to the equilibrium phase diagram but more consistent with the paraequilibrium estimates (Fig. 1).

Kinetic simulations

The experimental observations indicate that the microstructure obtained is inconsistent with equilibrium and that paraequilibrium solid state transformation may explain the excessive amount of austenite obtained. To confirm this, simulations have been conducted using DICTRA, capable of dealing with diffusional growth in

Table 2 Microanalytical results for manganese and aluminium (concentrations in wt-%)

	δ-Ferrite		Austenite	
	Mn	Al	Mn	Al
Equilibrium for 1612 K	1·95	2·52	3·77	1·15
Measured, Fig. 4*a*, region (i)	2·13±0·20	2·46±0·03	2·47±0·40	2·23±0·03
Measured, Fig. 4*b*, location 1	1·19±0·19	2·52±0·03		
Measured, Fig. 4*b*, locations 2 and 3			2·29±0·39	2·12±0·06
Measured, Fig. 4*b*, location 4			3·33±0·40	2·01±0·03

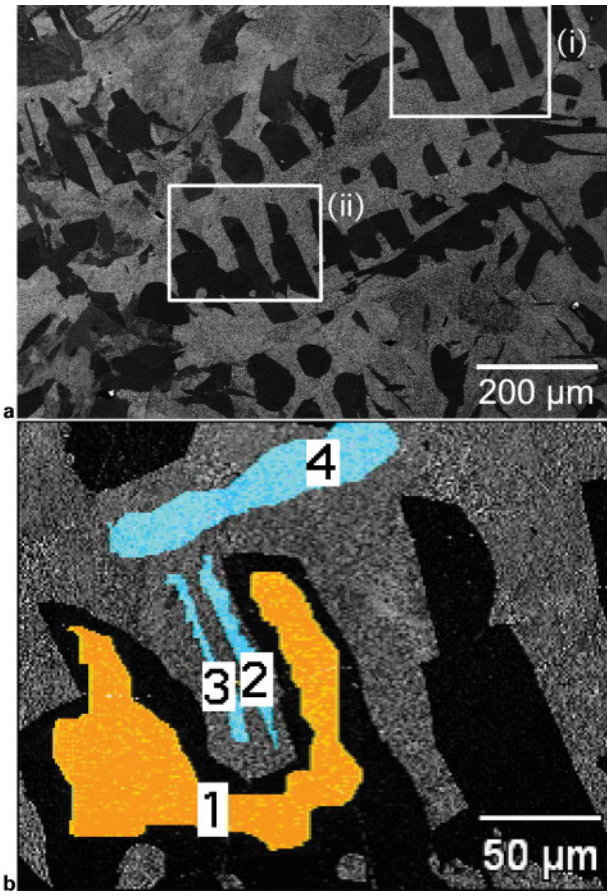

4 *a* Location of regions examined in detail and *b* Higher magnification of region (ii): orange marks region of δ-ferrite subjected to microanalysis, and blue marks austenite similarly analysed

multicomponent systems given the availability of thermodynamic and atomic mobility data.[29–32]

The scale of the microstructure selected for simulation is the approximate distance between δ-ferrite dendrites, i.e. 100 μm. Since the cooling rate of the 34 kg ingots used is not known, we have assumed a slow rate of 20 K s^{-1}, which is also a representative of many continuous casting operations.

Figure 7 shows simulations on the one-dimensional solidification of a 100 μm bar with the average composition of alloy 2. As expected, the austenite that forms during the course of solidification is rich in manganese and depleted in aluminium; this is consistent with the microanalytical data presented in Table 2 for location 4. Furthermore, the simulated concentrations averaged over the extent of this austenite are in reasonable quantitative agreement with the tabulated data for location 4.

The major discrepancy is that the amount of austenite that formed did not increase significantly beyond about 12% at 1500 K (see inset in Fig. 7*a*). The experiments described earlier suggest much larger austenite content. Allowing partitioning of all solutes does not therefore explain the observations even at the slow cooling rate used. To assess the alternative scenario that more austenite may form via a mechanism which does not result in the redistribution of substitutional solutes, a simulation was conducted on the limiting assumption that the δ-ferrite that remains at 1500 K is permitted to undergo paraequilibrium transformation into austenite. However, paraequilibrium transformation does not occur before approximately 1400 K is reached because of a lack of sufficient driving force.

To do this, the composition of the δ-ferrite was taken to be the average of that remaining at 1500 K to do a DICTRA paraequilibrium simulation. The simulation size was set to 40 μm to account for the reduced region available for further austenite to form, allowing for the fact that growth is expected from both the adjacent δ-ferrite regions. The composition used was therefore Fe–0·325C–0·21Si–1·8Mn–2·62Al (wt-%), and the computation was initiated with a thin (0·001 μm) layer of austenite of the same composition as the ferrite. The results shown in Fig. 8 are fascinating in that they prove that it is quite feasible for excess austenite to form at the slow cooling rate of 20 K s^{-1}.

It is emphasised again that the paraequilibrium calculation is a limiting, estimate since the real process can be anywhere between local equilibrium and local paraequilibrium.

The interpretation presented here explains not only the heterogeneous nature of the austenite by differentiating that which forms during solidification and the subsequent solid state transformation under conditions, where partitioning does not follow expectations from local equilibrium at the advancing interfaces.

Conclusions

The microscopic features of two alloys designed based on equilibrium to contain substantial amounts of δ-ferrite have been examined and found to display zero or much reduced fractions of this phase in the solidified condition. It is concluded that this is because the

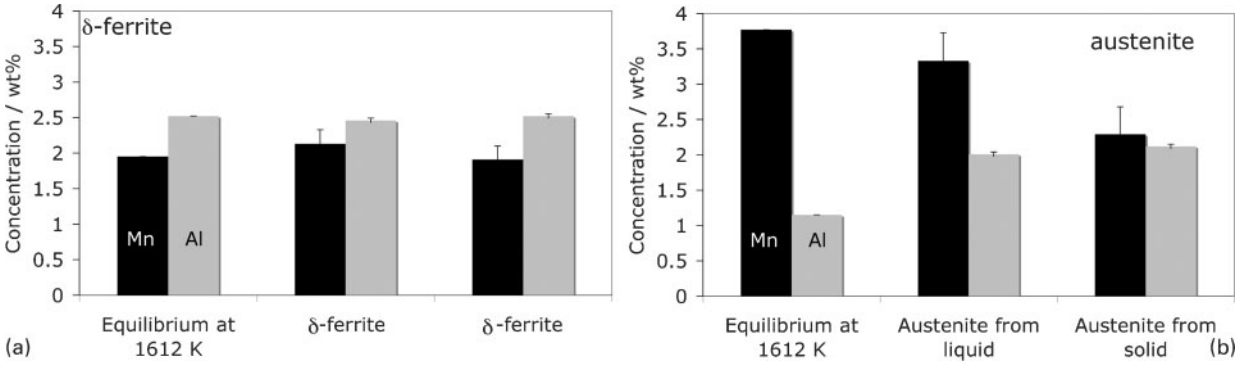

5 Illustration of data from Table 2

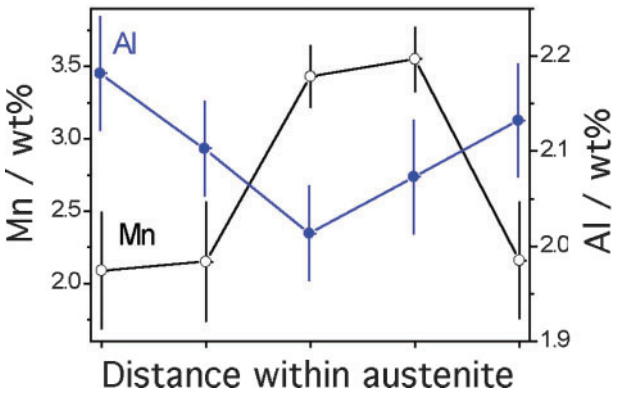

6 Microanalysis scan across core of austenite region in alloy 2: distance between successive microanalytical results is approximately 20 μm

austenite that forms during cooling by solid state transformation does so without the required partitioning of substitutional solutes. This is responsible for the diminished quantities of δ-ferrite found in the cast microstructures. This conclusion is supported by microanalytical data and through calculations of limiting phase diagrams based on paraequilibrium rather than equilibrium. Kinetic simulations support the conclusion that there are two stages involved in the formation of austenite: first, when the latter forms as part of the solidification process, and second, through solid state transformation of ferrite under circumstances where the substitutional solutes do not partition as expected from a local equilibrium condition at the transformation

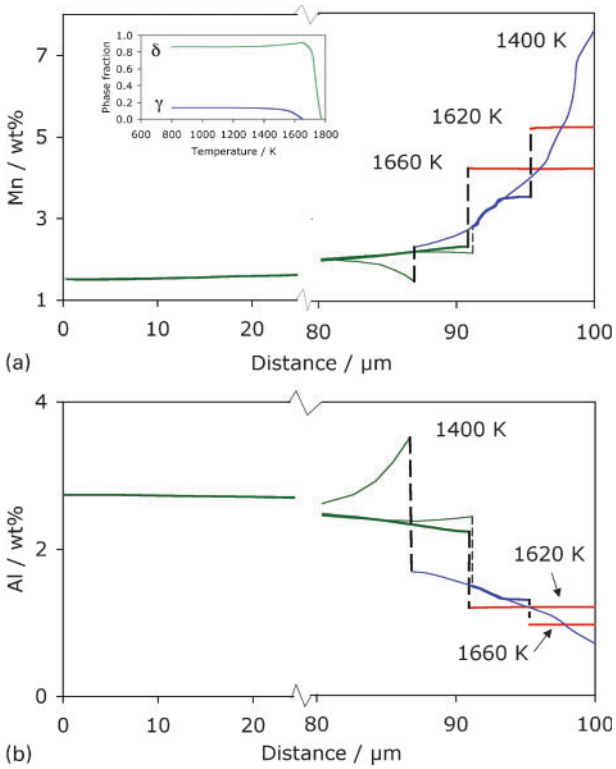

a distribution of manganese: inset shows how phase fractions evolve with time; *b* distribution of aluminium

7 Simulation of solidification of 100 μm bar at 20 K s^{-1} with cooling beginning from 1800 K: red represents liquid, green δ-ferrite and blue austenite; vertical broken lines represent interface positions

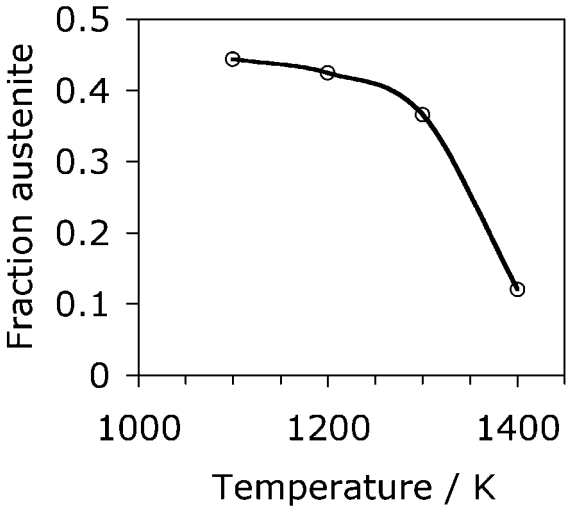

8 Kinetic calculation of austenite fraction as function of temperature

front. This explains the excessive amount of austenite obtained when compared with the equilibrium phase diagram.

Acknowledgement

The authors are grateful to Professor Hae-Geon Lee of the Graduate Institute of Ferrous Technology for the provision of laboratory facilities at POSTECH and to POSCO for help and support. Partly supported by World Class University Program Project R32-2008-000-10147-0.

References

1. B. C. DeCooman: *Curr. Opin. Solid State Mater. Sci.*, 2004, **8**, 285–303.
2. O. Matsumura, Y. Sakuma and H. Takechi: *Trans. Iron Steel Inst. Jpn*, 1987, **27**, 570–579.
3. O. Matsumura, Y. Sakuma and H. Takechi: *Scr. Metall.*, 1987, **27**, 1301–1306.
4. Y. Sakuma, O. Matsumura and H. Takechi: *Metall. Mater. Trans. A*, 1991, **22A**, 489–498.
5. Y. Sakuma, O. Matsumura and O. Akisue: *ISIJ Int.*, 1991, **31**, 1348–1353.
6. K. I. Sugimoto, A. Nagasaka, M. Kobayashi and S. I. Hashimoto: ISIJ Int., 1999, 39, 56–63.
7. P. J. Jacques: *Curr. Opin. Solid State Mater. Sci.*, 2004, **8**, 259–265.
8. S. Chatterjee and H. K. D. H. Bhadeshia: *Mater. Sci. Technol.*, 2007, **23**, 1101–1104.
9. S. Chatterjee and H. K. D. H. Bhadeshia: *Mater. Sci. Technol.*, 2006, **22**, 645–649.
10. H. K. D. H. Bhadeshia: *ISIJ Int.*, 2002, **42**, 1059–1060.
11. S. Chatterjee, M. Murugananth and H. K. D. H. Bhadeshia: *Mater. Sci. Technol.*, 2007, **23**, 819–827.
12. T. Kizu, Y. Nagataki, T. Inazumi and Y. Hosoya: *ISIJ Int.*, 2001, **41**, 1495–1501.
13. P. J. Jacques, E. Girault, P. Harlet and F. Delannay: *ISIJ Int.*, 2001, **41**, 1061–1067.
14. J. Deliry: *Mem. Sci. Rev. Metall.*, 1965, **62**, 527–550.
15. J. Pomey: *Mem. Sci. Rev. Metall.*, 1966, **63**, 507–532.
16. J. M. Schissler, J. Arnould and G. Metauer: *Mem. Sci. Rev. Metall.*, 1975, **72**, 779–793.
17. E. Kozeschnik and H. K. D. H. Bhadeshia: *Mater. Sci. Technol.*, 2008, **24**, 343–347.
18. A. G. Allten: *Trans. ASM*, 1954, **46**, 812–829.
19. E. W. Langer: *Met. Sci. J.*, 1968, **2**, 59.
20. M. S. Bhat: 'Microstructure and mechanical properties of AISI 4340 Steel modified with Al and Si', PhD thesis, Lawrence Berkeley Laboratories, Berkeley, CA, 1977.
21. NPL. MTDATA. Software, National Physical Laboratory, Teddington, UK, 2006.

22. A. Hultgren: *JKA-Jernkontoret. Ann.*, 1951, **135**, 403–494.
23. M. Hillert: *JKA-Jernkontoret. Ann.*, 1952, **136**, 25–37.
24. M. Hillert: 'Paraequilibrium', Technical report, Swedish Institute for Metals Research, Stockholm, Sweden, 1953.
25. H. I. Aaronson, H. A. Domian and G. M. Pound: *TMS-AIME*, 1966, **236**, 753–767.
26. H. I. Aaronson, H. A. Domian and G. M. Pound: *TMS-AIME*, 1966, **236**, 768–780.
27. H. I. Aaronson, H. A. Domian and G. M. Pound: *TMS-AIME*, 1966, **236**, 781–796.
28. H. K. D. H. Bhadeshia: *Prog. Mater. Sci.*, 1985, **29**, 321–386.
29. J. Ågren: *Scand. J. Metall.*, 1991, **20**, 86–92.
30. J. Ågren: *ISIJ Int.*, 1992, **32**, 291–296.
31. A. Engström, L. Höglund and J. Ågren: *Mater. Sci. Forum*, 1994, **163–166**, 725–730.
32. A. Borgenstam, A. Engström, L. Höglund and J. Ågren: *J. Phase Equilib.*, 2000, **21**, 269–280.